

# Wood as inspiration for new stimuli-responsive structures and materials

Joseph E. Jakes<sup>\*a</sup>, Nayomi Plaza<sup>ab</sup>, Samuel L. Zelinka<sup>c</sup>, Donald S. Stone<sup>bd</sup>, Sophie-Charlotte Gleber<sup>e</sup>, Stefan Vogt<sup>e</sup>

<sup>a</sup>Forest Biopolymers Science and Engineering, USDA Forest Service, Forest Products Laboratory, One Gifford Pinchot Drive, Madison, WI, USA 53726; <sup>b</sup>Materials Science Program, University of Wisconsin-Madison, 1509 University Ave., Madison, WI, USA 53706; <sup>c</sup>Durability and Wood Protection Research, USDA Forest Service, Forest Products Laboratory, One Gifford Pinchot Drive, Madison, WI, USA 53726; <sup>d</sup>Materials Science and Engineering, University of Wisconsin-Madison, 1509 University Ave., Madison, WI, USA 53706; <sup>e</sup>X-ray Science Division, Argonne National Laboratory, 9700 S. Cass Ave., Argonne, IL, USA 60439

## ABSTRACT

Nature has often provided inspiration for new smart structures and materials. Recently, we showed a bundle of a few wood cells are moisture-activated torsional actuators that can reversibly twist multiple revolutions per centimeter of length. The bundles produce specific torque higher than that produced by electric motors and possess shape memory twist capabilities. Here we also report that ion diffusion through wood cell walls is a stimuli-responsive phenomenon. Using the high spatial resolution and sensitivity of synchrotron-based x-ray fluorescence microscopy (XFM), metal ions deposited into individual wood cell walls were mapped. Then, using a custom-built relative humidity (RH) chamber, diffusion of the metal ions was observed *in situ* first at low RH and then at increasingly higher RH. We found that ions did not diffuse through wood cell walls at low RH, but diffusion occurred at high RH. We propose that both the shape memory twist effect and the moisture content threshold for ionic diffusion are controlled by the hemicelluloses passing through a moisture-dependent glass transition in the 60–80% RH range at room temperature. An advantage of wood over other stimuli-responsive polymers is that wood lacks bulk mechanical softening at the transition that controls the stimuli-responsive behavior. We demonstrate using a custom-built torque sensor that the torque generation in wood cell bundles actually continues to increase over the RH range that hemicelluloses soften. The hierarchical structure of wood provides the inspiration to engineer stimuli-responsive polymers and actuators with increased mechanical strength and higher recovery stresses.

**Keywords:** shape memory, torsional actuator, wood, stimuli-responsive diffusion

\*jjakes@fs.fed.us; phone 1 608 231-9308; fax 1 608 231-9592; [www.fpl.fs.fed.us](http://www.fpl.fs.fed.us)

## 1. INTRODUCTION

New stimuli-responsive structures and materials are sought for areas as diverse as drug delivery systems, deployable space structures, energy harvesting, sensors, and artificial muscles<sup>1–5</sup>. Stimuli-responsive materials are designed to respond to a variety of external stimuli, such as heat, solvent, light, moisture, or magnetic fields. Although moisture-activated actuations in plants have previously been studied with the motivation to inspire new stimuli-responsive materials and structures<sup>6–8</sup>, much of the previous work concentrated on only small, unidirectional movements such as opening of pine cones<sup>9</sup>, unfolding ice plant seed capsules<sup>10</sup>, wheat awn movements<sup>11</sup>, and bending of leaning tree organs<sup>12</sup>. Recently, we discovered that a bundle of a few loblolly pine (*Pinus taeda*) wood cells is a high specific torque actuator with large angle of rotation and shape memory twist capabilities<sup>13</sup>. Both the torsional actuation and shape memory twist effect are moisture-activated and derive from the hierarchical structure of wood. Individual wood cells, called tracheids, can be thought of as long hollow tubes typically 3–5 mm in length and 30–50 μm in diameter. The cell walls consist of helically wound semicrystalline cellulose microfibrils embedded in a matrix of amorphous cellulose, hemicelluloses, and lignin<sup>14</sup>. Cellulose is a linear polysaccharide, hemicelluloses are branched amorphous polysaccharides, and lignin is an amorphous aromatic polymer<sup>15</sup>. Individual wood cells are held together by the middle lamella, which consists of an open cellular hemicelluloses structure embedded with lignin. As the uptake of moisture

swells the amorphous wood polymers in the cell walls, the constraint from the helically wound cellulose microfibrils causes wood cells to twist<sup>16-17</sup>. The amount of twist in a cell bundle will depend on the helical angle of the cellulose microfibrils and the number of cells in the bundle<sup>18-19</sup>. In one of our bundles, which consisted of approximately five cells in cross section, we observed two revolutions per centimeter of length when the sliver was conditioned from 0 to 100% relative humidity (RH)<sup>13</sup>. The twisting was fully reversible during drying and repeatable.

Stimuli-responsive synthetic torsional actuators with helically wound reinforcement, similar to wood cells, have been reported, but none meets the performance of wood cell bundles. Torsional actuators using conjugated polymers have been demonstrated, but twisted less than 4° per centimeter of length<sup>20</sup>. Carbon nanotube yarn in electrolyte solutions<sup>21</sup> and wax-filled carbon nanotube yarn<sup>22</sup> torsional actuators twisted multiple revolutions per centimeter of length, but could not untwist without being coupled to return springs. Similarly, although carbon nanotube yarn torsional actuators produced high specific torques during twisting (2.4 N·m/kg for nanotube yarn in electrolyte solutions<sup>21</sup> and 8.4 N·m/kg for the wax-filled carbon nanotube<sup>22</sup>), they could not produce untwisting torques. Our wood cell bundle with approximately five cells in cross section produced 10 N·m/kg specific torque during both twisting and untwisting. For comparison, electric motors typically produce up to 6 N·m/kg specific torque<sup>23</sup>. The superior performance of the wood cell bundle suggests that much is still to be learned about optimal design of stimuli-responsive synthetic torsional actuators.

In addition to high angle of rotation and high specific torque, bundles of wood cells also exhibit a shape memory twist effect<sup>13</sup>. If the bundle is wetted and then constrained during drying, the majority of the twist is locked-in after constraint release. Upon rewetting and drying, the unconstrained bundle returns to its original twist. We also observed that a nanoindent impression in the middle lamella fully recovered after being wetted<sup>13</sup>. This observation meant that a good shape memory material can be made from lignin and hemicelluloses. Shape memory effects in polymers are usually controlled by property changes at a melting or glass transition<sup>1-2</sup>. Moisture-induced glass transition in hemicelluloses predominately occurs between 60% and 80% RH at room temperature<sup>24-26</sup>. In contrast, even for water-saturated wood, lignin glass transition is well above room temperature, at approximately 70°C<sup>27</sup>. Therefore, we concluded that moisture-dependent glass transition of hemicelluloses likely controls the shape fixing mechanism in wood cell bundles, and indeed in twist recovery experiments we observed the majority of the twist was unlocked over the 60–80% RH range<sup>13</sup>.

An advantage of wood over other stimuli-responsive actuators made from shape memory polymers is that wood does not experience the drastic bulk mechanical softening associated with the polymer crossing a melting or glass transition during shape fixing and recovery steps. The reported elastic modulus of shape memory polymers below the transition can be between 10 and 3000 MPa. However, above the transition, the polymers soften and elastic moduli are typically only between 0.1 and 10 MPa<sup>1</sup>. Consequently, recovery stresses are limited for shape memory polymer actuators and shape memory polymers have little, if any, potential to be used in load-bearing applications. In contrast, the decrease in wood elastic modulus associated with the hemicelluloses' glass transition is very weak<sup>24</sup>. The elastic modulus of bulk wood undergoes large mechanical softening at the lignin glass transition, which occurs well above room temperature even for water-saturated wood<sup>27</sup>. It is uncertain, however, what impact the hemicelluloses' glass transition has on the torque generated by the cell bundle. In our previous work, we assessed only the overall specific torque generated as the bundle was conditioned from 0 to 100% RH or 100% to 0 RH. In this proceeding, cell bundles were conditioned at multiple RH steps between 0 and 100% in both adsorption and desorption to investigate if the hemicelluloses' mechanical softening in the 60–80% RH range impacts cell bundle torque generation.

The large amount of twist recovery occurring in the 60–80% RH range in wood cell bundles suggests that in this RH range, large interconnecting regions of softened hemicelluloses are being formed. Large interconnected regions are likely formed through percolation of smaller regions. Recently, we proposed that large interconnecting regions of softened hemicelluloses facilitate long-range chemical transport within wood cell walls<sup>28</sup>. This proposal is also supported by fitting impedance measurements to a percolation model with the threshold for ionic conduction set at 16% moisture content, which occurs when wood is conditioned at approximately 75% RH at room temperature<sup>29</sup>. In this context, wood cell walls are also stimuli-responsive materials for chemical transport, which could inspire new drug delivery systems. In this proceeding, initial experiments showing a moisture threshold for diffusion of Cu ions in wood cell walls are reported. The experiment utilizes the high spatial resolution and sensitivity of synchrotron-based x-ray fluorescence microscopy (XFM).

## 2. MATERIALS AND METHODS

### 2.1 Torque sensor

Commercial torque sensors could not be found to reliably assess the small torque (less than  $10^{-7}$  N·m) generated during moisture-induced twisting of cell wall bundles. We therefore designed and built torque sensors that were inspired by the sensitive torsional pendulums used by Coulomb<sup>30-32</sup> and Cavendish<sup>33</sup> in their fundamental measurements of the electrostatic force constant and gravitational force constant, respectively. The torque sensors used 63.5- $\mu$ m-diameter tungsten wires from Metal Cutting Corporation (Cedar Grove, NJ, USA). Miniaturized connectors were constructed using plates machined from 0.4-mm-thick brass sheets and bolted together with brass screws and nuts (thread size 00-90) from J.I. Morris Company (Southbridge, MA, USA) (**Figure 1a**).

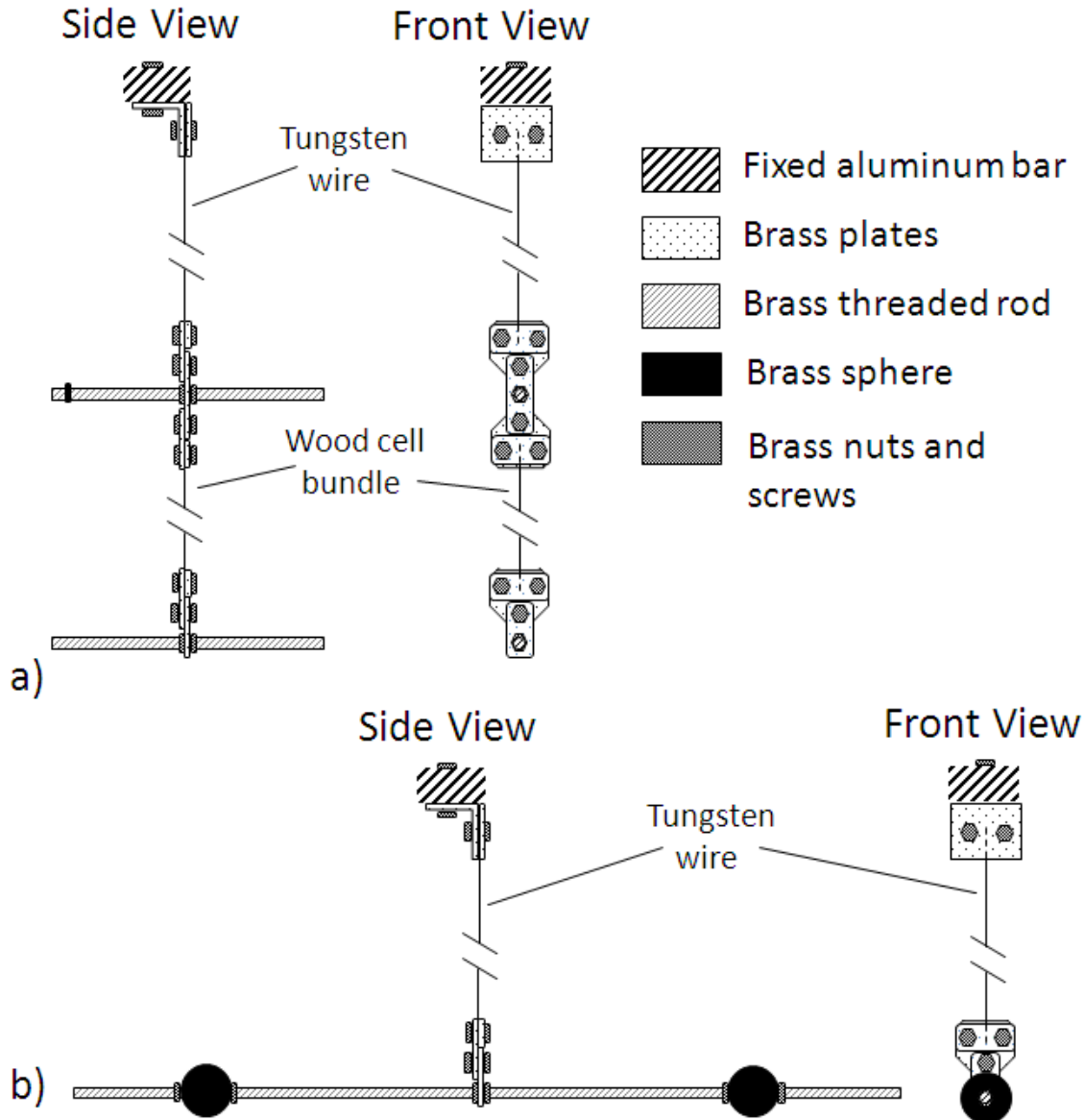


Figure 1. Sketches of a) connector design for tungsten wires and cell bundles, and b) dumbbell mass for torsional pendulums. The spheres were 4.76-mm-diameter brass and threaded to screw onto the 74-mm-long threaded rod (brass, thread size 00-90, obtained from J.I. Morris Company (Southbridge, MA, USA)). Five dumbbells were constructed using  $r_1 = 6.4, 12.7, 17.8, 25.4,$  or  $34.3$  mm.

The torsional stiffness  $k$  of a round wire is given by

$$k = \frac{G\pi d^4}{32L} \quad (1)$$

where  $G$  is shear modulus (161 GPa for tungsten),  $d$  is wire diameter, and  $L$  is wire length. Torque  $T$  can then be calculated from

$$T = k\theta \quad (2)$$

where  $\theta$  is twist in radians. To validate the  $k$  of the tungsten wire used in the torque sensors, experiments were performed to calculate the tungsten  $G$  and compared to the literature value of 161 GPa. Experiments consisted of measuring natural frequencies of oscillation of 15 torsional pendulums made from combinations of attaching one of five dumbbell-shaped masses to one of three lengths of wire. Details of the dumbbell masses are given in **Figure 1b**. The natural frequency of each torsional pendulum was measured by perturbing it and analyzing digital movies of the oscillations. Natural frequency  $\omega$  of a torsional pendulum is governed by

$$\omega = \sqrt{\frac{k}{I}} = \sqrt{\frac{G\pi d^4}{32LI}} \quad (3)$$

where  $I$  is moment of inertia of the attached mass. For each dumbbell,

$$I_i = I_{\text{rod}} + 2mr_i^2 \quad (4)$$

where  $I_{\text{rod}}$  is the moment of inertia of the rod,  $m$  is the sphere mass and two nuts that secured the sphere on the threaded rod (see **Figure 2b**),  $r_i$  is half the distance between the sphere centers, and  $i = 1$  to 5 representing one of the five dumbbell masses. For our dumbbell masses, we include contributions of the connecting plates and bolts into  $I_{\text{rod}}$ . Therefore,  $I_{\text{rod}}$  cannot be calculated simply and is an unknown. However, we assume it is a constant for all five masses because rod length and connectors were all the same. The following analysis was used to assess  $G$  using only the known wire diameter, wire lengths, sphere mass, distance between spheres, and measured natural frequencies.

Squaring Equation 3 gives

$$\omega^2 = \frac{G\pi d^4}{32I} \left( \frac{1}{L} \right) \quad (5)$$

For each dumbbell mass  $\omega^2$  plotted against  $L^{-1}$  is a linear relationship as shown in **Figure 2**.

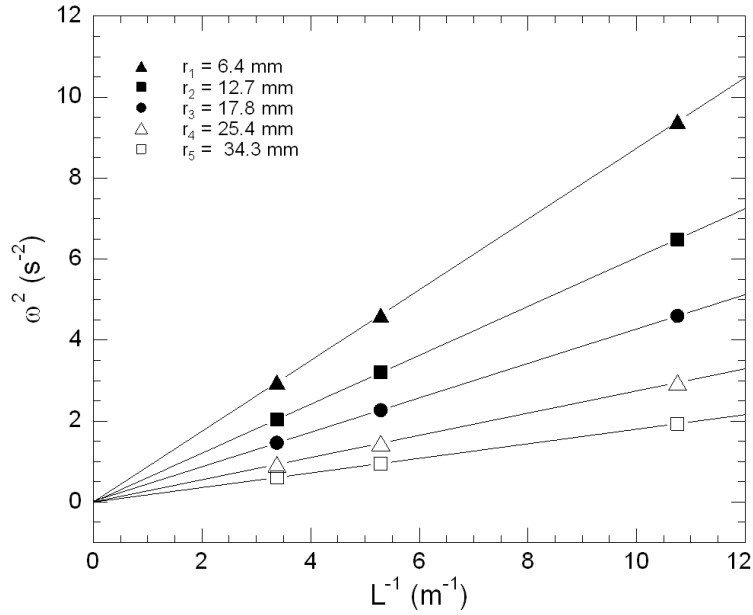


Figure 2. Linear relationship between natural frequency squared ( $\omega^2$ ) and inverse wire length ( $L^{-1}$ ) for each dumbbell mass based on Equation 5.

The slope  $m_i$  of each linear fit in **Figure 2** is  $G\pi d^4/(32L_i)$ . Taking the slope ratio of  $m_1$  to  $m_i$  and using Equation 4 gives

$$\frac{m_1}{m_i} = \frac{\frac{G\pi d^4}{32LL_1}}{\frac{G\pi d^4}{32LL_i}} = \frac{I_i}{I_1} = \frac{I_{\text{rod}}}{I_1} + \frac{2mr_i^2}{I_1} \quad (6)$$

From Equation 6, a plot of  $m_1/m_i$  vs.  $r_i^2$  is linear with a slope equal to  $2m/I_1$  (**Figure 3**).

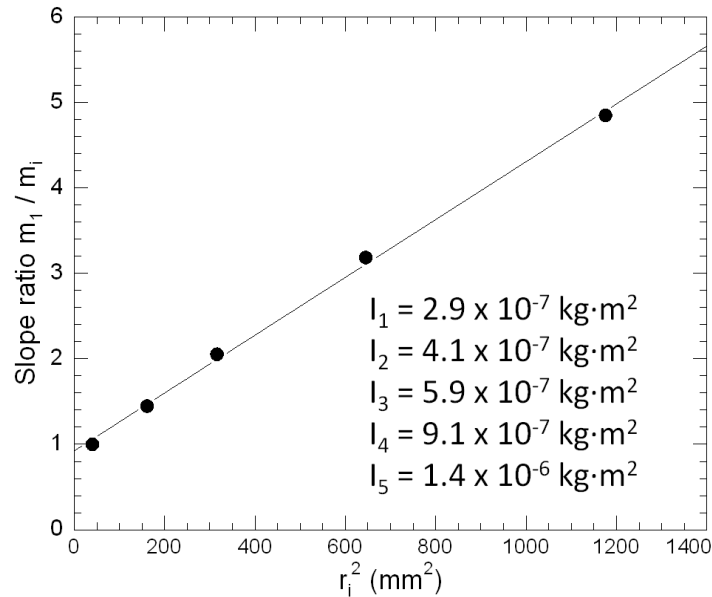


Figure 3. Relationship between slope ratio ( $m_1/m_i$ ) and the square of half the distance between the sphere centers ( $r_i^2$ ) following Equation 6.

Using the slope of the linear relationship in **Figure 3** and known sphere mass (0.44 g), the value of  $I_1$  can be calculated from Equation 6. Then, using the  $m_1/m_i$  ratio and Equation 6,  $I_i$  for  $i = 2$  to 4 can be calculated. For each of the 15 configurations,  $G$  was then calculated by rearranging Equation 5. The result was  $G = 157 \pm 1$  GPa (uncertainty one standard deviation), which is within 3% of the 161 GPa literature value.

In addition to validating the tungsten wire torsional stiffness, these experiments also provide five dumbbell masses with known moments of inertia that can be used in future experiments with wood cell bundles, the advantage being that they can easily be placed inside a glove box attached to cell wall bundles. With the known moment of inertia, natural frequency could be calculated as a function of RH conditioning. Then, with knowledge of cell bundle diameter,  $G$  can be assessed. Additionally, the generation of  $T$  during twisting can also be studied in the future through the equation  $T = Ia$  where  $a$  is angular acceleration.

## 2.2 Specific torque of moisture-induced sliver twisting

Previously established methods were used to make a wood cell bundle approximately 50  $\mu\text{m}$  in diameter extracted from latewood loblolly pine<sup>13</sup>. One end of the cell bundle was connected to the end of a 10.2 cm length of 63.5- $\mu\text{m}$ -diameter tungsten wire ( $k = 2.3 \times 10^{-6}$  N-m/rad) using the setup illustrated in **Figure 1a**. The torque sensor was set up inside a Plexiglas<sup>®</sup> glove box in which RH was controlled by an InstruQuest HumiSys<sup>™</sup> HF (Coconut Creek, FL, USA) RH generator. After conditioning the bundle in lab-supplied compressed air (3% RH) for 10 h, the bundle free end was fixed by constraining the bottom rod with a stack of Al bars. A digital photograph was taken to identify the starting position of the rod between the cell bundle and tungsten wire. Then, the bundle was conditioned for 10 h each at eight RH steps up to 94% RH and then 10 h each at eight RH steps back down to 3% RH. Time-lapse photography was used to ensure that the wood bundle stopped twisting, and the final image was used to measure change in twist at each step. To calculate specific torque, first the volume of the bundle was estimated using cross-section area measured from scanning electron microscopy images post-experiment and bundle length. Then, mass of the bundle was calculated using 0.6 g/cm<sup>3</sup> as the specific gravity of loblolly pine latewood<sup>34</sup>.

## 2.3 X-ray fluorescence microscopy (XFM)

In XFM, x-rays are focused onto a sample and incident x-rays can be absorbed by an atom. Absorbed x-rays typically lead to the ejection of an inner-shell electron for sufficiently high incident energy. For medium- to high-Z elements, the relaxation of an outer-shell electron typically fills the inner-shell vacancy and results in the emission of a fluorescence photon that has energy characteristic of the element. The fluorescence photons are then detected with an energy dispersive detector to assess the type and amount of element present in the spot illuminated by the focused x-ray beam. Maps of elements in a specimen can then be built up point by point by raster scanning the focused x-ray beam over regions of interest<sup>35-37</sup>. We used synchrotron-based XFM at beamline 2-ID-E at the Advanced Photon Source at Argonne National Laboratory (Argonne, IL, USA) to monitor metal ion diffusion in wood cell walls as a function of RH conditioning. For the experiments, 2- $\mu\text{m}$ -thick longitudinal-tangential latewood loblolly pine sections were cut using a diamond knife fit into a Sorvall (Norwalk, Connecticut, USA) MT-2 ultramicrotome. The wood sections were then secured over the hole in a copper StrateTek<sup>™</sup> 1/1 mm double folding TEM grid from Ted Pella Inc. (Redding, CA, USA). Ions were implanted into a small region of the wood section using a small droplet of copper sulfate saturated salt solution using a micropipette connected to a XenoWorks<sup>™</sup> Digital Microinjector (Sutter, Novato, CA). An optical microscopy image of the droplet on the wood section is shown in **Figure 4**. The wood section was then fit into a custom-built RH chamber in the beamline. The RH was controlled by a HumiSys<sup>™</sup> relative humidity generator (Instruquest, Coconut Creek, FL). The temperature and relative humidity inside of the chamber was continuously monitored by a Sensirion (Staeafa, Switzerland) SHT1x sensor. A 10.2-keV x-ray beam was focused into a spot approximately 0.8 by 0.5  $\mu\text{m}$ . Elemental maps were built over the indicated area in **Figure 4** using 0.3- $\mu\text{m}$  step sizes with 5-ms dwell times at each step. Images were obtained at 42, 52, 55, 60, 65, 71, 75, 80, 85, 90, and 95% RH. At each RH step the chamber was given approximately 30 min to equilibrate and was maintained at the RH for the approximately 60 min needed to obtain the image. Data analysis was carried using the MAPS software package<sup>38</sup>. In brief, full spectra were fit to modified Gaussian peaks, the background was iteratively calculated and subtracted, and results were compared to standard reference materials (NBS 1832 and 1833, NIST). A more detailed manuscript describing ion diffusion in wood cell walls is forthcoming<sup>39</sup>, and only initial results demonstrating that wood cell walls are stimuli-responsive chemical transport materials are given here.

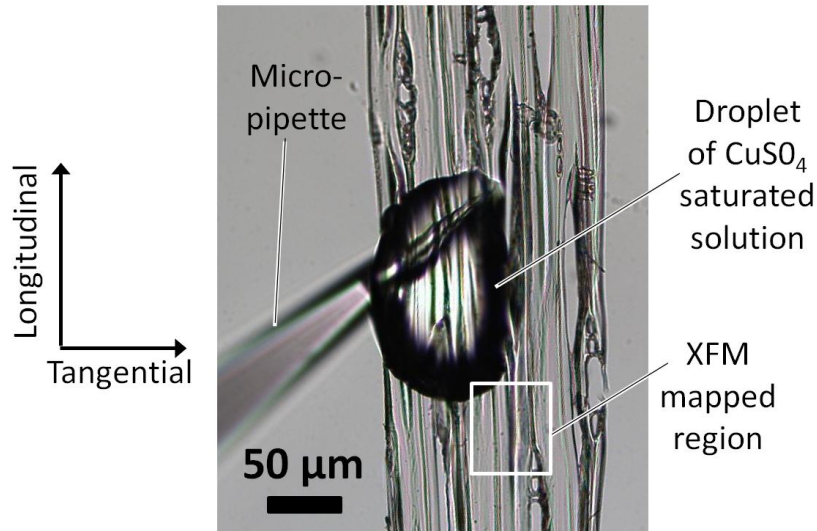


Figure 4. Optical microscopy image of the droplet of  $\text{CuSO}_4$  saturated solution used to implant Cu ions in a 2- $\mu\text{m}$ -thick longitudinal-tangential section of latewood loblolly pine. The region mapped with XFM is indicated.

### 3. RESULTS

#### 3.1 Torque generation during moisture-induced wood cell bundle twisting

The specific torque generated during moisture-induced twisting and untwisting of a wood cell bundle is shown in **Figure 5**. When conditioned from 3% to 94% RH, this bundle produced 25  $\text{N}\cdot\text{m}/\text{kg}$  specific torque, which is much higher than our previously reported bundle that produced 10  $\text{N}\cdot\text{m}/\text{kg}$  specific torque<sup>13</sup>. This higher specific torque suggests that more detailed work is needed to find the optimal cell bundle design to produce the highest specific torque possible. Also included in **Figure 5** are typical moisture sorption isotherms taken from loblolly pine<sup>40</sup>. Both specific torque and sorption isotherms continuously increase with RH, and their similar shapes suggest that torque is strongly related to moisture content. However, the hysteresis in the torque isotherms is different than the hysteresis in the sorption isotherms. The hysteresis is much smaller and, in contrast to the moisture sorption isotherms, specific torque in adsorption lies above specific torque in desorption. Also indicated in **Figure 5** is the 60–80% RH region over which hemicelluloses mechanically soften as they undergo a moisture-induced glass transition<sup>24–26</sup>. Specific torque continually increases through this region, meaning mechanical softening of the hemicelluloses does not impact the generation of torque in wood cell bundles.

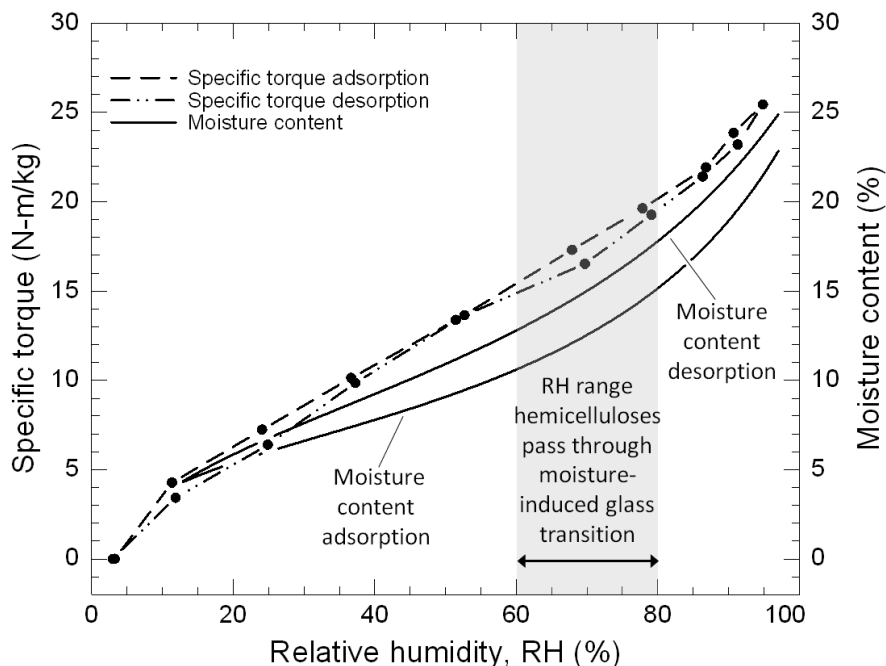


Figure 5. Specific torque generated during relative humidity (RH) conditioning as assessed by the custom-built torque sensor in **Figure 1a**. Also included are moisture sorption isotherms taken from loblolly pine<sup>40</sup>. Moisture content is defined as water mass divided by oven-dried wood mass.

In the shape memory twist effect in wood cell bundles, the hemicelluloses' glass transition is believed to control the shape fixing mechanism. Typical shape memory polymers undergo mechanical softening above their shape fixing and shape recovery transition and, as a result, have very small recovery forces. In contrast, wood does not undergo mechanical softening as the hemicelluloses' pass through their glass transition<sup>24</sup>, and based on the results in **Figure 5**, it would be expected that wood cell bundles are also capable of producing large recovery torques when the hemicelluloses are mechanically softened during shape fixing and recovery. This improved performance likely results from the effective incorporation of stiff cellulose microfibrils into the matrix of the hemicelluloses and lignin, although the complex cellular structure of wood may also be contributing. Through further study of the hierarchical structure of wood, inspiration should emerge to build polymer-based stimuli-responsive actuators with improved mechanical properties and higher recovery stresses.

### 3.2 Moisture threshold for ion transport in wood cell walls

XFM images from the specified region in **Figure 4** are given in **Figures 6a-l**. All the figures are Cu maps except for the Zn map in **Figure 6a**. The Zn mapped in **Figure 6a** is naturally occurring, and because Zn has a higher concentration in the middle lamellae than in the cell wall<sup>41</sup>, it can be used to help identify the middle lamella in the XFM maps. The areas between and to the outside of the middle lamellae are secondary cell walls. The high concentration of Cu in the upper left hand corners in **Figures 6b-l** is the region implanted by the droplet shown in **Figure 4**. In the initial Cu XFM map at 42% RH, a sharp boundary of the implanted region is observed in the cell walls and middle lamella. For RH steps below 65% RH, no obvious diffusion of Cu can be observed. However, beginning at 65% RH, some fuzziness at the interface appears and in subsequent images Cu movement can be observed first in the middle lamella and then in the cell walls. By 95% RH, Cu ions have spread throughout the map. Unfortunately, the RH control was not perfect and the RH values with an asterisk after them experienced an RH spike while the image was being made, as described in the figure caption. Nevertheless, the threshold for ionic diffusion appears to be in the same 60–80% RH range that also corresponds to the range over which hemicelluloses go through their moisture-induced glass transition.

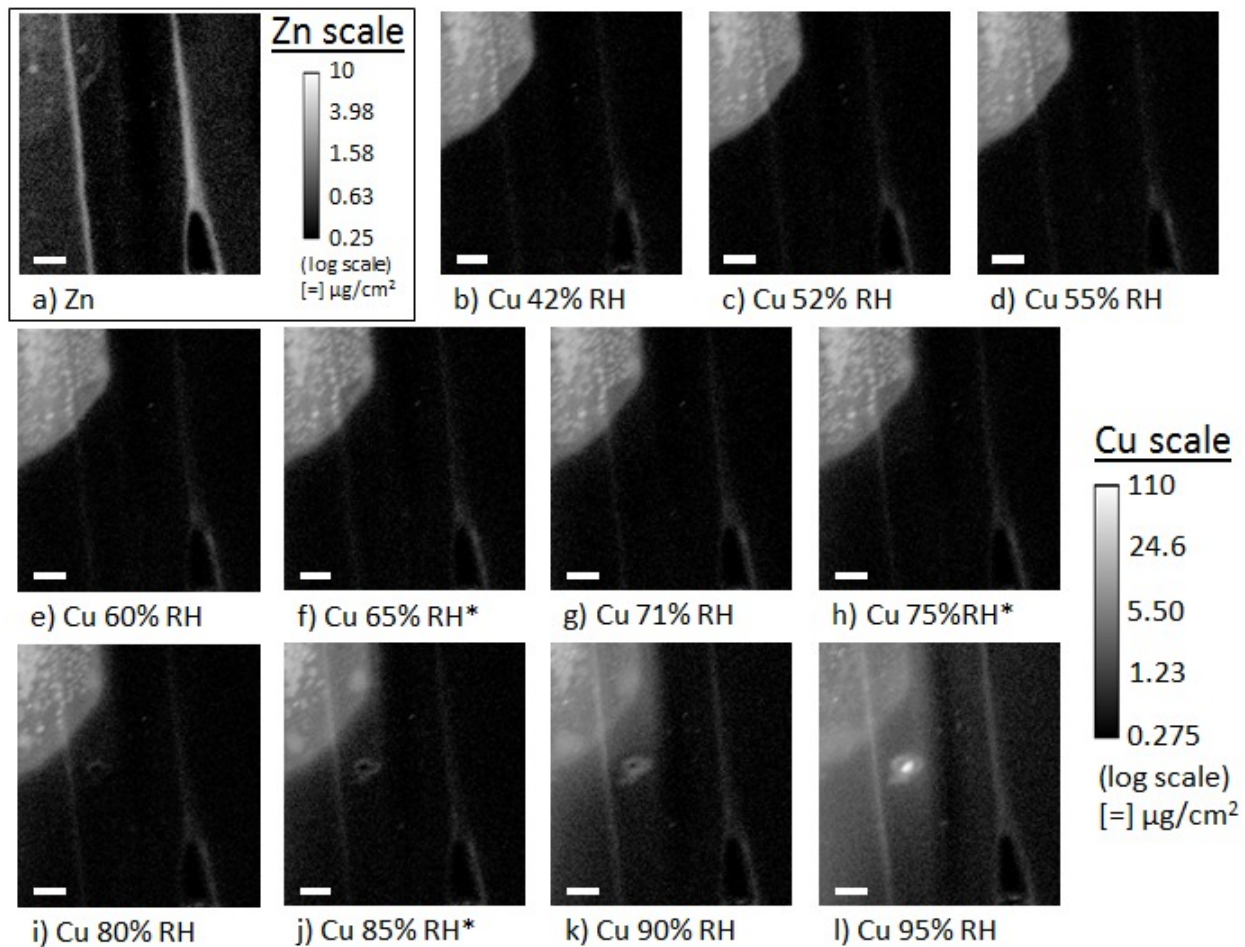


Figure 6. X-ray fluorescence microscopy (XFM) maps of a) Zn and b–l) Cu after relative humidity (RH) conditioning. RH values denoted by \* experienced the following RH spikes during the imaging: 65% RH – 70% RH spike for 15 min; 75% RH – 78% RH spike for 1 min; 85%RH – 87% RH spike for 1 min. (scale bar = 10  $\mu\text{m}$ )

We recently proposed that long-range chemical transport through wood cell walls occurs through percolated regions of hemicelluloses mechanically softened after passing through their moisture-induced glass transitions<sup>28</sup>. A schematic of the cell wall nanostructure illustrating this mechanism is shown in **Figure 7**. The cell wall nanostructure is not fully known but is believed to consist of cellulose microfibrils coated with hemicelluloses and oriented in the longitudinal cell direction. The region between cellulose microfibrils also contains lignin and additional hemicelluloses regions. As the cell wall begins to absorb moisture, regions of hemicelluloses pass through moisture-induced glass transitions and mechanically soften. At the percolation moisture content, regions of mechanically softened hemicelluloses connect to exceed a percolation threshold so continuous diffusion channels are formed to facilitate long-range chemical transport. The moisture threshold for ionic diffusion through wood cell walls observed by XFM (**Figure 6**) provides strong evidence to confirm the recently proposed mechanism for long-range chemical transport through wood cell walls<sup>28</sup> and the percolation model of electrical conduction in wood<sup>29</sup>.

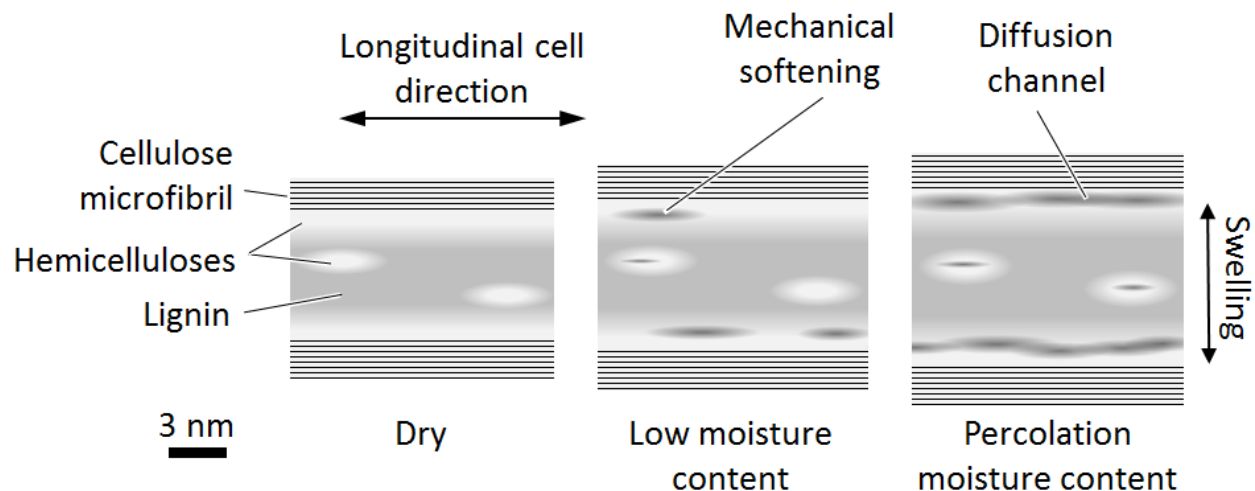


Figure 7. Schematic of cell wall nanostructure showing moisture sorption causing regions of hemicelluloses to soften and then percolate to form diffusion channels.

#### 4. DISCUSSION

Potential applications for wood cell bundles or wood-inspired synthetic materials and structures are numerous. When cell bundles are exposed to changes in RH, they twist in direct proportion to RH producing high specific torque. The bundles can twist revolutions per centimeter of length in a few seconds when directly wetted or in 10s of seconds when exposed to step changes in RH. These are favorable characteristics for stimuli-responsive torsional micro actuators. Because of their small size they also reach equilibrium within a few minutes, making cell bundles a responsive and inexpensive RH sensor. Using the moisture-induced twist recovery factor previously studied<sup>13</sup>, a system could also be designed to serve as a long-term peak RH sensor that acts passively and could be used in remote places. Additionally, a system could be designed to harvest energy from twisting bundles if they are placed in an environment that experiences regular changes in RH.

Opportunities also exist to use inspiration from wood to improve other torsional actuators being developed. For instance, wood cell walls may provide a solution for carbon nanotube yarn-based torsion actuators to overcome their lack of ability to return to their original form without return springs. In both electrolyte-driven and wax-filled yarns, expansion of material between the helically wound carbon nanotube yarns causes twist, but nothing is inherent in the system to remember its original configuration. In wood cell walls, lignin serves this function and remembers its original configuration and provides the returning forces. Lignin is basically a cross-linked amorphous polymer capable of absorbing water. A cross-linked matrix material that can expand when exposed to stimulation might be more appropriate than wax- or electrolyte-based systems. The cell wall could be further simulated by perhaps first coating the carbon nanotubes with a material that could mimic the hemicelluloses and provide a shape fixing mechanism within the carbon nanotube yarn as well.

One primary advantage of wood over other stimuli-responsive polymers (e.g., shape memory polymers and controlled drug release polymers) is that wood maintains its mechanical strength over the full range of operating conditions. In wood, both the shape memory twist effect and onset of ion diffusion are likely controlled by mechanical softening of the hemicelluloses. However, because of the nanostructure of wood cell wall there is little bulk mechanical softening of wood associated with the hemicelluloses softening. Apparently, cellulose microfibrils and lignin are capable of maintaining wood strength when wet. Wood could therefore provide inspiration for a new type of drug delivery system. The drug could be implanted into a material that is stiff enough to push into tissue. Once inside the tissue, the material could be stimulated to release the drug over a prescribed period of time. But by maintaining its mechanical strength the device could then be wholly withdrawn from the tissue after treatment.

## 5. CONCLUSIONS

Wood continues to provide new inspiration for stimuli-responsive materials and structures. Bundles of wood cell walls are moisture-activated torsional actuators capable of high angles of rotation, high specific torque, and shape memory twist effects. Additionally, chemical transport through wood cell walls is moisture-responsive. The origins of these behaviors derive from the complex hierarchical wood structure that spans from the molecular-scale up to cell bundles in the work presented here. There is strong evidence the shape memory effects and moisture threshold of ionic diffusion are controlled by the hemicelluloses being mechanically softened as they pass through a moisture-induced glass transition. However, despite the hemicelluloses component softening, wood does not undergo a drastic mechanical softening. Therefore, in contrast to other shape memory polymers, wood bundles can maintain their mechanical strength during shape fixing and recovery steps. Also, the generation of torque over the RH range that hemicelluloses soften is found to be unaffected by the hemicelluloses softening. The combination of mechanical properties and stimuli-responsive behavior is very interesting and should inspire improved or new stimuli-responsive structures and materials.

## ACKNOWLEDGEMENTS

JEJ and SLZ acknowledge funding from 2011 and 2010 USDA PECASE awards, respectively. NP acknowledges the GERS program at UW–Madison and 2012 NSF GFRP for support. JEJ and NP acknowledge support from the FHA Cooperative Research Program for Covered Timber Bridges. The use of Advanced Photon Source facilities was supported by the US Department of Energy, Basic Energy Sciences, Office of Science, under contract number W-31-109-Eng-38. Tom Kuster in the Analytical Chemistry and Microscopy Laboratory at FPL is acknowledged for SEM images used to assess the bundle cross-section diameter.

## REFERENCES

- [1] Liu, C., Qin, H., and Mather, P.T., “Review of progress in shape-memory polymers,” *J. Mater. Chem.* 17(16), 1543–1558 (2007).
- [2] Mather, P.T., Luo, X.F., and Rousseau, I.A., “Shape memory polymer research,” *Annu. Rev. Mater. Res.* 39, 445–471 (2009).
- [3] Stuart, M.A.C., Huck, W.T.S., Genzer, J., Müller, M., Ober, C., Stamm, M., Sukhorukov, G.B., Szleifer, I., Tsukruk, V. V., et al., “Emerging applications of stimuli-responsive polymer materials,” *Nat. Mater.* 9(2), 101–113 (2010).
- [4] Mano, J.F., “Stimuli-Responsive Polymeric Systems for Biomedical Applications,” *Adv. Eng. Mater.* 10(6), 515–527 (2008).
- [5] De Las Heras Alarcon, C., Pennadam, S., and Alexander, C., “Stimuli responsive polymers for biomedical applications,” *Chem. Soc. Rev.* 34(3), 276–85 (2005).
- [6] Fratzl, P., and Barth, F.G., “Biomaterial systems for mechanosensing and actuation,” *Nature* 462(7272), 442–448 (2009).
- [7] Burgert, I., and Fratzl, P., “Actuation systems in plants as prototypes for bioinspired devices,” *Philos. Trans. R. Soc. A Math. Physical Eng. Sci.* 367(1893), 1541–1557 (2009).
- [8] Martone, P.T., Boller, M., Burgert, I., Dumais, J., Edwards, J., Mach, K., Rowe, N., Rueggeberg, M., Seidel, R., et al., “Mechanics without muscle: biomechanical inspiration from the plant world,” *Integr. Comp. Biol.* 50(5), 888–907 (2010).
- [9] Dawson, C., Vincent, J.F. V., and Rocca, A.-M., “How pine cones open,” *Nature* 390(6661), 668 (1997).
- [10] Harrington, M.J., Razghandi, K., Ditsch, F., Guiducci, L., Rueggeberg, M., Dunlop, J.W.C., Fratzl, P., Neinhuis, C., and Burgert, I., “Origami-like unfolding of hydro-actuated ice plant seed capsules,” *Nat. Commun.* 2, 337 (2011).
- [11] Elbaum, R., Zaltzman, L., Burgert, I., and Fratzl, P., “The role of wheat awns in the seed dispersal unit,” *Science* (80-. ). 316(5826), 884–886 (2007).
- [12] Burgert, I., Eder, M., Gierlinger, N., and Fratzl, P., “Tensile and compressive stresses in tracheids are induced by swelling based on geometrical constraints of the wood cell,” *Planta* 226(4), 981–987 (2007).

- [13] Plaza, N., Zelinka, S.L., Stone, D.S., and Jakes, J.E., "Plant-based torsional actuator with memory," *Smart Mater. Struct.* 22(7), 072001 (2013).
- [14] Wiedenhoeft, A.C., [Structure and Function of Wood] , in *Handb. Wood Chem. Wood Compos.*, R. M. Rowell, Ed., CRC Press, Boca Raton, 9–32 (2013).
- [15] Rowell, R.M., Petterson, R., and Tshabalala, M.A., [Cell Wall Chemistry] , in *Handb. Wood Chem. Wood Compos.*, R. M. Rowell, Ed., CRC Press, Boca Raton, FL, 33–72 (2013).
- [16] Gillis, P.P., and Mark, R.E., "Analysis of shrinkage, swelling and twisting of pulp fibers," *Cellul. Chem. Technol.* 7, 209–234 (1973).
- [17] Stanzl-Tschegg, S., "Properties of chemically and mechanically isolated fibres of spruce (*Picea abies* [L.] Karst.). Part 2: Twisting phenomena," *Holzforschung* 59(2), 247–251 (2005).
- [18] Gray, D.G., and Kam, A., "Chiral characteristics of thin wood sections," *Holzforschung* 51(1), 1–5 (1997).
- [19] Schulgasser, K., and Witztum, A., "The hierarchy of chirality," *J. Theor. Biol.* 230(2), 281–288 (2004).
- [20] Fang, Y., Pence, T., and Tan, X., "Fiber-directed conjugated-polymer torsional actuator: nonlinear elasticity modeling and experimental validation," *IEEE/ASME Transactions on Mechatronics* 16(4), 656–664 (2011).
- [21] Foroughi, J., Spinks, G.M., Wallace, G.G., Oh, J., Kozlov, M.E., Fang, S., Mirfakhrai, T., Madden, J.D.W., Shin, M.K., et al., "Torsional carbon nanotube artificial muscles," *Science* (80-. ). 334(6055), 494–497 (2011).
- [22] Lima, M.D., Li, N., Jung de Andrade, M., Fang, S., Oh, J., Spinks, G.M., Kozlov, M.E., Haines, C.S., Suh, D., et al., "Electrically, Chemically, and Photonically Powered Torsional and Tensile Actuation of Hybrid Carbon Nanotube Yarn Muscles," *Science* (80-. ). 338(6109), 928–932 (2012).
- [23] Hollerbach, J.M., Hunter, I.W., and Ballantyne, J., [A comparative analysis of actuator technologies for robotics] , in *Robot. Rev.* 2, O. Khatib, J. Craig, and P. Lozano, Eds., MIT Press, Cambridge, MA, 299–342 (1991).
- [24] Kelley, S.S., Rials, T.G., and Glasser, W.G., "Relaxation behaviour of the amorphous components of wood," *J. Mater. Sci.* 22(2), 617–624 (1987).
- [25] Cousins, W.J., "Young's modulus of hemicellulose as related to moisture content," *Wood Sci. Technol.* 12(3), 161–167 (1978).
- [26] Olsson, A.-M., and Salmén, L., [The softening behavior of hemicelluloses related to moisture] , in *Hemicellul. Sci. Technol.* 864(864), P. Gatenholm and M. Tenkanen, Eds., American Chemical Society, Washington, 184–197 (2003).
- [27] Salmén, L., "Viscoelastic properties of in situ lignin under water-saturated conditions," *J. Mater. Sci.* 19(9), 3090–3096 (1984).
- [28] Jakes, J., Plaza, N., Stone, D., and Hunt, C., "Mechanism of Transport Through Wood Cell Wall Polymers," *J. For. Prod. Ind.* 2(6), 10–13 (2013).
- [29] Zelinka, S., Glass, S., and Stone, D., "A percolation model for electrical conduction in wood with implications for wood-water relations," *Wood Fiber Sci.* 40(4), 544–552 (2008).
- [30] Coulomb, C.-A., "Premier mémoire sur l'électricité et le magnétisme," *Mémoires l'Académie R. des Sci.* 569–577 (1785).
- [31] Coulomb, C.-A., "Second mémoire sur l'électricité et le magnétisme," *Mémoires l'Académie R. des Sci.* 578–611 (1785).
- [32] Magie, W.F., [Coulomb: Law of Electric Force] , 8th ed., in *A Source B. Phys.*, 8th ed., Harvard University Press, Cambridge, ed. 8, 408–417 (1963).
- [33] Cavendish, H., "Experiments to determine the density of the earth," *Philos. Trans. R. Soc. London* 88, 469–526 (1798).
- [34] Cramer, S., Kretschmann, D., Lakes, R., and Schmidt, T., "Earlywood and latewood elastic properties in loblolly pine," *Holzforschung* 59(5), 531–538 (2005).
- [35] Fittschen, U.E.A., and Falkenberg, G., "Trends in environmental science using microscopic X-ray fluorescence," *Spectrochim. Acta Part B At. Spectrosc.* 66(8), 567–580 (2011).
- [36] Paunesku, T., Vogt, S., Maser, J., Lai, B., and Woloschak, G., "X-ray fluorescence microprobe imaging in biology and medicine," *J. Cell. Biochem.* 99(6), 1489–502 (2006).
- [37] Twining, B.S., Baines, S.B., Fisher, N.S., Maser, J., Vogt, S., Jacobsen, C., Tovar-Sanchez, A., and Sañudo-Wilhelmy, S.A., "Quantifying Trace Elements in Individual Aquatic Protist Cells with a Synchrotron X-ray Fluorescence Microprobe," *Anal. Chem.* 75(15), 3806–3816 (2003).
- [38] VOGT, S., "MAPS: A set of software tools for analysis and visualization of 3D X-ray fluorescence data sets," *J. Phys. IV* 104, 635–638 (2003).

- [39] Zelinka, S.L., Gleber, S.-C., Vogt, S., and Jakes, J.E., "The threshold for ion movement in wood cell walls below fiber saturation observed by micro X-ray fluorescence spectroscopy," Unpublished.
- [40] Zelinka, S.L., and Glass, S. V., "Water vapor sorption isotherms for southern pine treated with several waterborne preservatives," *ASTM J. Test. Eval.* 38, 80–88 (2010).
- [41] Saka, S., and Goring, D., "The distribution of inorganic constituents in black spruce wood as determined by TEM-EDXA," *J. Japan Wood Res. Soc.* 29(10), 648–656 (1983).